A Stratified, Lineage-Agnostic Analysis of Persulfide-Related Protein Expression and Erastin Resistance Across Cancer Cell Lines

Ömer Ekmel Kara

June 2025

1.0 Table of Content & Abbreviations

Abbreviations	
AIFM2	Apoptosis-Inducing Factor Mitochondrion-Associated 2 (also known as FSP1)
BH	Benjamini–Hochberg
CBS	Cystathionine β-Synthase
CSE/CTH	Cystathionine γ-Lyase
ETHE1	Ethylmalonic Encephalopathy Protein 1
FC	Fold Change
FDR	False Discovery Rate
FSP1	Ferroptosis Suppressor Protein 1 (also known as AIFM2)
GPX4	Glutathione Peroxidase 4
LR	Linear Regression
MLR	Multiple Linear Regression
MPST	Mercaptopyruvate Sulfurtransferase
PRDX	Peroxiredoxin
R^2	Coefficient of Determination
RSSH	Reactive Sulfur Species (Persulfides)
SCLY	Selenocysteine Lyase
SLR	Simple Linear Regression
SQR	Sulfide:Quinone Oxidoreductase
TST	Thiosulfate Sulfurtransferase
VIF	Variance Inflation Factor
xCT/SLC7A	Solute Carrier Family 7 Member 11 (Cystine/Glutamate Antiporter)

2.0 Background

Ferroptosis is a form of regulated cell death characterized by lipid peroxidation via iron dependent Fenton reaction. Cancer cells often develop resistance to ferroptosis through various antioxidant defence pathways, including glutathione peroxidase 4 (GPX4), ferroptosis suppressor protein 1 (FSP1, also known as AIFM2), and more recently, persulfide-producing enzymes such as cystathionine β-synthase (CBS) (Erdélyi et al., 2021; Berndt et al., 2024). However, few studies have systematically investigated how the expression levels of these genes influence ferroptosis sensitivity by utilizing current large-scale datasets.

In this study, two independendent DepMap datasets were used to explore potential correlations between relative resistance to erastin—a known direct XCt and indirect GPX4 inhibitor and ferroptosis inducer—and the expression of four proteins known for persulfide-synthesis and ferroptosis inhibitory effect in different models: XCt/SLC7A11, CBS, thiosulfate sulfurtransferase (TST), and mercaptopyruvate sulfurtransferase (MPST). Additionally, the effects of GPX4 and FSP1/AIFM2 expression were assessed to better understand the role of persulfide synthesizing enzymes in ferroptosis resistance in context dependent manner.

Elucidating the interplay between these antioxidant mechanisms with erastin sensitivity in various cancer cell lines may generate initial insights which may reveal key common pathways and the relationship between persulfide biology and ferroptosis, potentially guiding future targeted investigations.

3.0 Introduction

Ferroptosis is a non-apoptotic form of cell death driven by iron-dependent lipid peroxidation, leading to plasma membrane rupture. Though fundamentally a spontaneous chemical process, its execution is strongly influenced by various metabolic and redox-regulatory pathways (Berndt et al., 2024). Several of these pathways present promising targets for therapeutic intervention in degenerative diseases and cancers. Small-molecule electrophilic agents such as RSL3 (a GPX4 inhibitor) and erastin have been used to induce ferroptosis; however, their therapeutic utility is limited due to reasons such as high toxicity and the capacity of cancer cells to activate alternative ferroptosis resistance mechanisms, some of which remain poorly understood (Zhang et al., 2022; Diao et al., 2024).

AIFM2 has been firmly established as a key independent regulator of ferroptosis resistance, functioning in parallel to GPX4 across diverse cellular contexts (Berndt et al., 2024). In contrast, while antioxidant enzymes such as PRDX1 and PRDX6 contribute to redox homeostasis through detoxification of reactive oxygen species—and PRDX6 may additionally support selenoprotein biosynthesis—there is no compelling evidence that they can functionally compensate for the genetic loss of GPX4 in a universal manner (Adamiec-Organisciok et al., 2023; Lu et al., 2019; Chen et al., 2024). Unlike AIFM2, which rescues GPX4-deficient cells via its NAD(P)H-dependent CoQ10 regeneration pathway, PRDX family members lack a similarly robust, GPX4-independent mechanism for broad ferroptosis suppression. As demonstrated in Chen et al. (2024), deletion of PRDX6, SCLY, and LRP8 sensitizes cells to ferroptosis when GPX4 is present but has no effect in a GPX4-deficient, AIFM2-reliant context—underscoring their supportive rather than essential roles outside the GPX4 axis.

Parallel to these insights, recent studies have shown that cysteine availability also impacts ferroptosis sensitivity independently of GPX4 (Zhang et al., 2023). Overexpression of xCT, the cystine/glutamate antiporter, shown to be able to complement the loss of GPX4—a phenomenon linked to increased

production of endogenous persulfide species such as GSSH and GSSSH (Barayeu et al., 2022). These species are also upregulated under pro-ferroptotic conditions, suggesting that enhanced persulfide biosynthesis forms part of an adaptive defense against lipid peroxidation. Furthermore, the anti- and pro-ferroptotic roles of CSE (also known as CTH) and ETHE1, respectively, along with contributions from other enzymes like CBS, MPST, and CARS, highlight a broader metabolic axis influencing ferroptosis via regulation of reactive sulfur species (Wu et al., 2023). For example, CBS depletion sensitizes breast cancer cells to ferroptosis without altering GSH or cysteine levels, indicating that its role in H_2S and persulfide production is functionally significant (Kimura et al., 2021).

Together, these findings illustrate a multifaceted regulatory network wherein both CoQ10-driven antioxidant systems (GPX4, AIFM2) and RSSH-related sulfur metabolism impact ferroptosis sensitivity. However, most of these studies were conducted in a restricted subset of cancer cell lines, often limited to specific tissue origins, and therefore do not capture global trends across diverse cancer lineages. This study aims to highlight the lineage-independent (global) relevance of persulfide-synthesizing enzymes, which have previously been shown to correlate with ferroptosis resistance in context-dependent settings.

Accordingly, this study focused exclusively on GPX4 and FSP1 expression for cellular subgroup stratification and as independent variables in linear and multiple regression models comparing erastin sensitivity to protein levels—both due to their well-validated, non-redundant mechanisms and to ensure clarity in model interpretation. Five beforementioned key persulfide-producing enzymes were included as additional variables based on their emerging relevance, providing a biologically grounded framework for understanding cell-type-specific ferroptosis vulnerabilities.

4.0 Methods and Experimental Design

Erastin resistance was operationally defined as the $\log_2$ fold change in cell viability after erastin treatment, sourced from the PRISM Repurposing Public 24Q2 dataset. Protein expression profiles of the specific cell lines were sourced from the DepMap Harmonized MS CCLE Gygi proteomics dataset (Corsello et al., 2020; Nusinow et al., 2020).

Although the "All samples" model provides an overall view of the relationship between protein expression and Erastin resistance across the full dataset, it may mask context-specific effects due to biological heterogeneity. To address this, stratified subgroup analyses were performed based on GPX4 and AIFM2 expression levels. While these subgroups share overlapping samples and are therefore not fully independent, they offer valuable insight into how protein-resistance associations may shift under differing ferroptotic regulatory states. These stratified models are not intended to replicate the global analysis, but rather to decompose it into condition-specific contexts.

Only cell lines which were present in both datasets were used for the statistical analysis. Cell lines were independently categorized into subgroups based on the $\log_2$ fold change (FC) expression levels of two known ferroptosis inhibitors: GPX4 and FSP1 (AIFM2):

- High expression ($\log_2$ FC > 1)
- Low expression ($\log_2$ FC between -1 and 1)
- Negligible expression ($\log_2$ FC < -1)
- Both GPX4 and AIFM2 expression low ($\log_2$ FC < 0)

- All(full cell set)

Protein expression levels of GPX4, AIFM2, and the four persulfide-synthesizing enzymes (SLC7A11, CBS, TST, MPST) were correlated with erastin sensitivity (log_2 FC) within these subgroups using the same proteomics dataset.

Statistical analyses included simple correlation and linear regression (LR) analysis, and multiple linear regression (MLR) models to evaluate the effect of gene expression on erastin resistance. Subgroup-specific analyses were conducted to assess context-dependent associations. Data parsing and normalization were performed in Python, while all regression modeling and visualization were carried out in R. Portions of the text and code were edited using ChatGPT-4. The hypotheses, statistical methodologies, and interpretation of results were conceived and executed only by the author. Complete datasets, additional analyses, and scripts are provided in the Supplementary Data File. Further details are described in the "Statistical Methods" section.

4.1 Statistical Methods

4.1.1 Analytical Strategy

Prior to constructing multiple linear regression (MLR) models, parsimonious correlation and simple linear regression (SLR) analyses were conducted to assess the independent associations between Erastin resistance and each gene of interest within relevant expression-defined subgroups. This step ensured that only candidate predictors with evidence of individual correlation were retained for MLR modeling. Sample sizes were not normalized across subgroups, and each model was treated independently to preserve biological stratification.

CBS was excluded from MLR analyses, as no significant positive correlation with Erastin resistance was observed in any subgroup. In contrast, each of the remaining persulfide-related genes—SLC7A11, TST, and MPST—demonstrated a significant or near-significant correlation in at least one context.

Due to a strong positive correlation between TST and MPST expression (Pearson's $r \approx 0.5$; see Fig. 3A & B), MLR models were designed to include only one of these proteins within a model to avoid multicollinearity. Model performance was evaluated using Pearson correlation coefficients for SLRs and R^2 values for MLRs. Only statistically significant associations ($p < 0.05$) or those trending toward significance ($0.05 < p < 0.1$) are reported in figures.

To maintain model robustness and interpretability across variable sample sizes (n = 24–270), a parsimonious modeling strategy was employed. For subgroups with fewer than 50 samples, models were limited to a maximum of three predictors to mitigate overfitting and multicollinearity risks. In larger subgroups, inclusion of additional predictors was justified by greater degrees of freedom and model stability.

4.1.2 Data Preparation

Data preprocessing and analysis were performed using the R statistical software (version 4.4.3). Key packages utilized included:

- tidyverse for data manipulation and visualization
- broom for tidying model outputs
- car for calculating Variance Inflation Factor (VIF)

- relaimpo for assessing relative importance of predictors
- openxlsx for exporting results to Excel

The main outcome variable was the log2 fold change in Erastin resistance, denoted as *Y*. Predictor variables included protein expression levels of GPX4, CBS, SLC7A11, TST, MPST, and AIFM2, denoted as $X_1, X_2, ..., X\_p$.

4.1.3 Simple Linear Correlation Analyses

For each protein, Pearson and Spearman correlation coefficients with erastin resistance were calculated within each condition. Results were visualized with scatterplots and linear regression lines to illustrate trends.

4.1.4 Multiple Linear Regression (MLR)

Multiple linear regression models were used to assess the association between protein expression levels and Erastin resistance. The general model is:

Equation 1:
$Y_i = \beta_o + \beta_1 X_{i1} + \beta_2 X_{i2} + ... + \beta\_p X_{ip} + \varepsilon_i$, for i = 1, ..., n

where:

- Y_i = log2 fold change in Erastin resistance for sample i
- X_{ij} = expression level of protein j in sample i
- β_o = intercept
- β_j = regression coefficient for predictor j
- ε_i = error term (assumed normal)

Models were run separately for biologically relevant subsets based on GPX4 and AIFM2 expression, categorized into "high," "low," "negligible", “both low” and “all" groups.

Model Diagnostics

- Variance Inflation Factor (VIF) was calculated for each predictor to assess multicollinearity; values above 5 indicate potential issues.
- Model fit was evaluated using R-squared and adjusted R-squared.
- To account for multiple hypothesis testing, all *p*-values from regression coefficients were adjusted using the Benjamini–Hochberg (BH) false discovery rate (FDR) correction.

  Equation 2:
  $p_i(adj) = \min\{(p_i \times m) / i, 1\}$

  p_i = original p-value

  m = total number of tests

  i = rank of p-value in ascending order

4.1.5 Relative Importance of Predictors

The relative contribution of each predictor to the explained variance (R^2) was assessed using the "lmg" method from the *relaimpo* package:

Equation 3:
$R\delta(j) = RIj \times R^2$

$R\delta(j) = \Delta R$= contribution of predictor j to the total explained variance

RIj= Average increase in R^2 when adding predictor j to all possible predictor subsets

R^2 =the total variance explained by the full model.

5. Figures and Tables

Table 1. Results of Correlation and Linear Regression Analyses Between Erastin Resistance and Protein Expression of SLC7A11, TST, MPST, GPX4, and AIFM2
Only statistically significant results ($p < 0.05$) and strong trends ($0.05 < p < 0.1$) are shown.

Correlation and Linear Regression of Erastin Resistance vs. Protein Expression							
Protein	Condition	Points	Pearson	Spearman	Slope	Intercept	P_value
GPX4	low GPX4	212	0,170703	0,108153	0,37584	0,064955	0,012807
GPX4	high AIFM2	45	0,307412	0,261792	0,405235	0,450514	0,039957
GPX4	negligible AIFM2	41	0,569001	0,541986	0,764954	-0,60447	0,000104
GPX4	all	276	0,139917	0,132059	0,181979	0,043962	0,020052
AIFM2	low GPX4	209	0,250701	0,243411	0,261901	0,043722	0,000251
AIFM2	both low	58	0,308895	0,311698	0,559776	0,067216	0,018311
AIFM2	all	270	0,166771	0,171667	0,168498	0,017018	0,006017
TST	low GPX4	212	0,177667	0,145377	0,19987	0,016169	0,009535
TST	negligible GPX4	39	0,326156	0,307692	0,390794	-0,25206	0,042728
TST	high AIFM2	45	0,26501	0,221476	0,253894	0,084706	0,078523
TST	low AIFM2	184	0,161699	0,129996	0,190758	0,055569	0,028315
TST	both low	58	0,264479	0,144606	0,407435	-0,27105	0,04483
TST	all	276	0,176312	0,140419	0,197318	0,000356	0,003294
SLC7A11	both low	53	0,266186	0,353653	0,29854	-0,4271	0,054033
SLC7A11	all	258	0,139501	0,132386	0,134368	-0,02525	0,025038
MPST	low GPX4	212	0,156526	0,092293	0,243611	0,046907	0,022628
MPST	high AIFM2	45	0,365439	0,380896	0,534783	0,228202	0,013568
MPST	all	276	0,162451	0,115622	0,249975	0,033412	0,006839

A

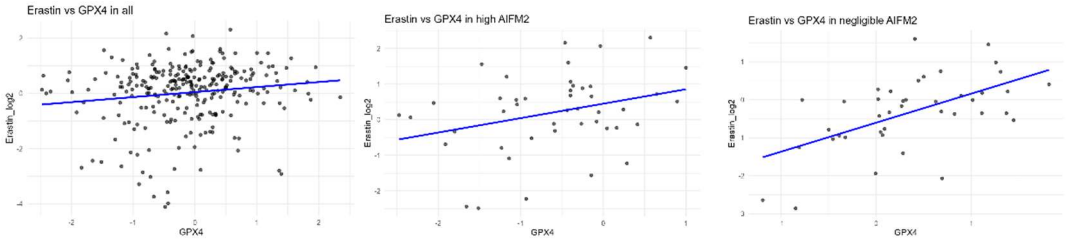
Erastin vs GPX4 in all
Erastin vs GPX4 in high AIFM2
Erastin vs GPX4 in negligible AIFM2
Erastin_log2
GPX4

B

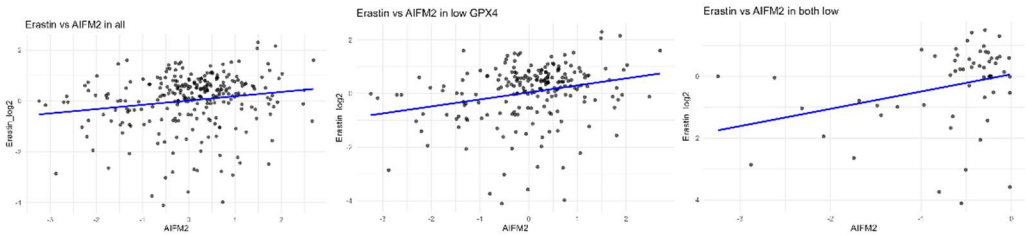
Erastin vs AIFM2 in all
Erastin vs AIFM2 in low GPX4
Erastin vs AIFM2 in both low
Erastin_log2
AIFM2

C

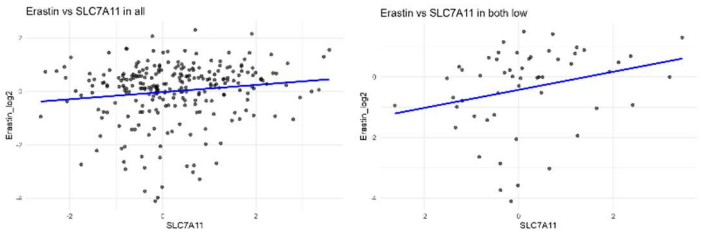
Erastin vs SLC7A11 in all
Erastin vs SLC7A11 in both low
Erastin_log2
SLC7A11

D

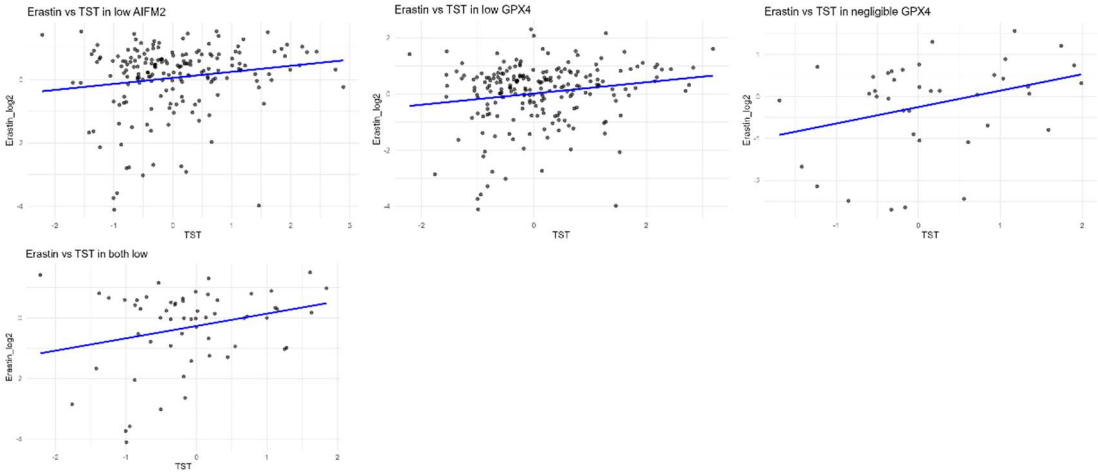
Erastin vs TST in low AIFM2
Erastin vs TST in low GPX4
Erastin vs TST in negligible GPX4
Erastin vs TST in both low
Erastin_log2
TST

E

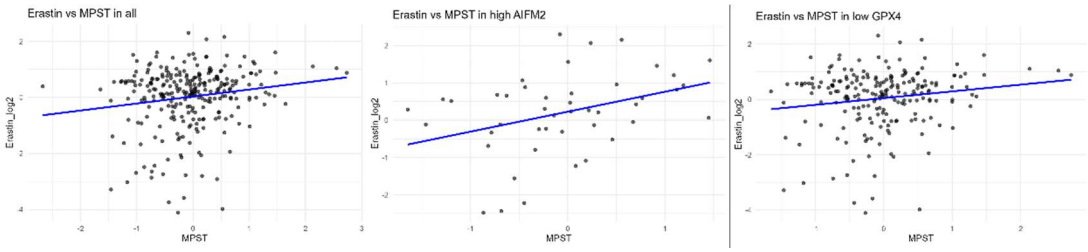
Erastin vs MPST in all
Erastin vs MPST in high AIFM2
Erastin vs MPST in low GPX4
Erastin_log2
MPST

Figure 1. Corelation and SLR analyses scatterplots showing the relationships between Erastin resistance (log_2 fold change) and protein expression levels of (A) GPX4, (B) AIFM2, (C) SLC7A11, (D) TST, and (E) MPST. These plots correspond to the statistical analyses summarized in Table 1.

A

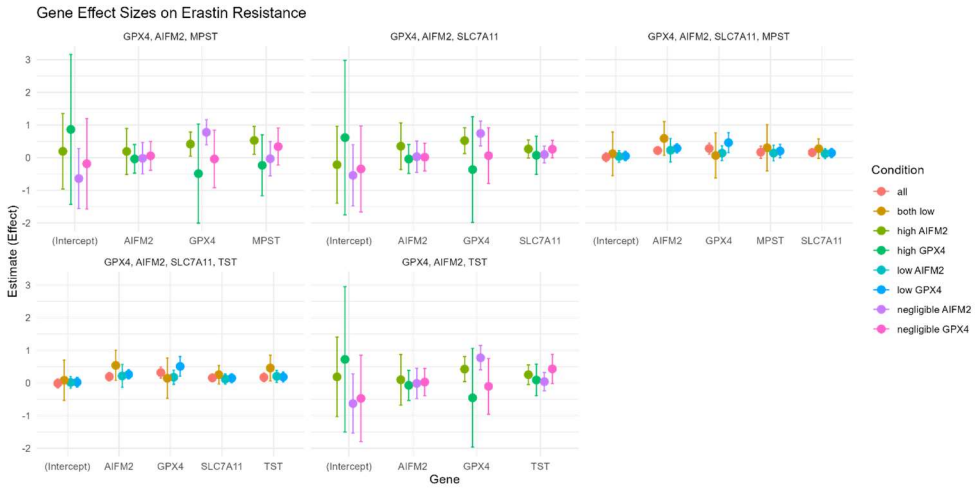

B

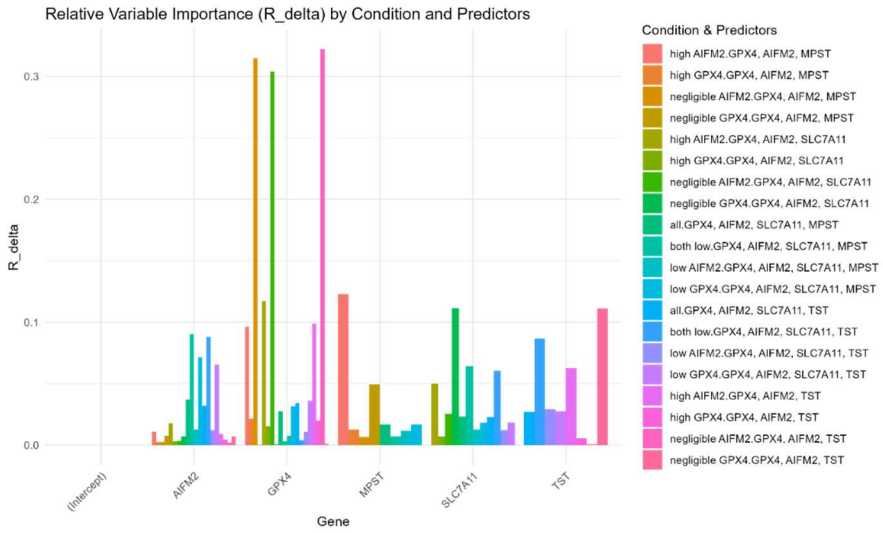

C

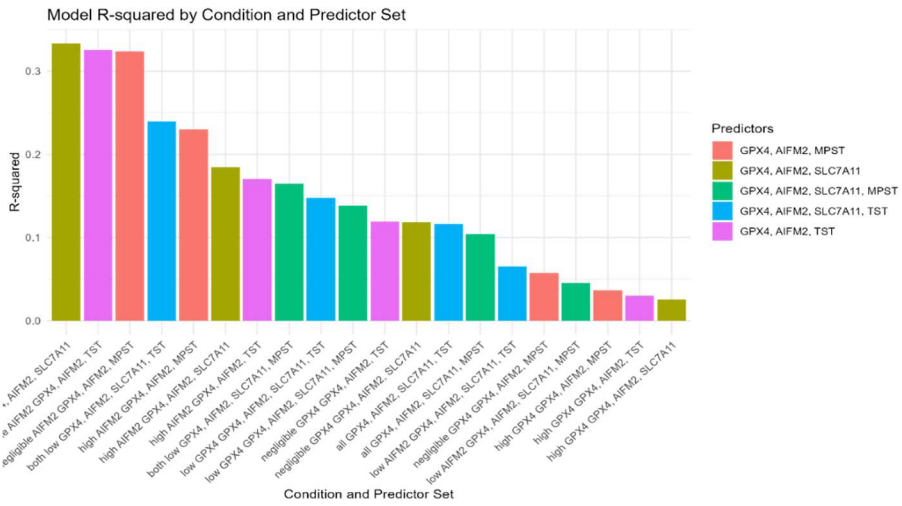

Figure 2. Statistical analysis of two multiple linear regression (MLR) models to highlight relationships between Erastin resistance and protein expression levels of SLC7A11, TST, MPST, GPX4, and AIFM2(refer to Table 2-6 for numerical statistic values). (A) Coefficient plot of MLR models showing the estimated effect sizes (β) of each gene on Erastin resistance across predictor set-condition-specific datasets. Each point represents the regression coefficient for a protein, with error bars indicating the 95% confidence intervals (CI). (B) R delta (ΔR) values representing the relative contribution of selected genes expression to the model's explanatory power, calculated by comparing the full model to reduced models excluding the respective gene. (C) Adjusted R^2 values for each MLR model by condition, representing the proportion of variance in Erastin resistance explained by the model.

Table 2. Multiple Linear Regression (MLR) analysis results for Erastin resistance models using SLC7A11, TST, MPST, GPX4, and AIFM2 as independent variables in Low GPX4 cell subsets. Red and Green cells highlight unique combination of condition and predictor set which represents an independent model.

Low GPX4 Cell Set Multiple Linear Regression Models for Erastin Resistance vs Protein Expression of Ferroptosis Inhibitors and Known Persulfide Synthesizing Enzymes															
Protein	estimate	std.error	statistic	p.value	Adjusted_P	R_squared	Adj_R_squared	R_delta	AIC	BIC	conf.low	conf.high	Condition	SampleSize	Predictors
GPX4	0,506297	0,153567	3,296901	0,001169	0,002922023	0,147648	0,129512706	0,036244	561,1012	580,6774	0,20336	0,809234	low GPX4	193	GPX4, AIFM2, SLC7A11, TST
AIFM2	0,260284	0,071167	3,657358	0,000331	0,00165373	0,147648	0,129512706	0,065477	561,1012	580,6774	0,119895	0,400673	low GPX4	193	GPX4, AIFM2, SLC7A11, TST
SLC7A11	0,146567	0,07065	2,074544	0,039391	0,049238586	0,147648	0,129512706	0,018434	561,1012	580,6774	0,007198	0,285935	low GPX4	193	GPX4, AIFM2, SLC7A11, TST
TST	0,182631	0,076988	2,372188	0,018693	0,031154969	0,147648	0,129512706	0,027493	561,1012	580,6774	0,030759	0,334503	low GPX4	193	GPX4, AIFM2, SLC7A11, TST
GPX4	0,45575	0,153448	2,970056	0,003366	0,008414566	0,13846	0,120129386	0,03181	563,1705	582,7467	0,153048	0,758451	low GPX4	193	GPX4, AIFM2, SLC7A11, MPST
AIFM2	0,283627	0,071048	3,992055	9,38E-05	0,000469244	0,13846	0,120129386	0,071602	563,1705	582,7467	0,143473	0,42378	low GPX4	193	GPX4, AIFM2, SLC7A11, MPST
SLC7A11	0,141758	0,071089	1,994098	0,047587	0,075805947	0,13846	0,120129386	0,018109	563,1705	582,7467	0,001524	0,281992	low GPX4	193	GPX4, AIFM2, SLC7A11, MPST
MPST	0,199077	0,105476	1,88742	0,060645	0,075805947	0,13846	0,120129386	0,016939	563,1705	582,7467	-0,00899	0,407144	low GPX4	193	GPX4, AIFM2, SLC7A11, MPST

Table 3. Multiple Linear Regression (MLR) analysis results for Erastin resistance models using SLC7A11, MPST, GPX4, and AIFM2 as independent variables in High AIFM2 cell subsets. Red and Blue cells highlight unique combination of condition and predictor set which represents an independent model.

High AIFM2 Cell Set Multiple Linear Regression Models for Erastin Resistance vs Protein Expression of Ferroptosis Inhibitors and Known Persulfide Synthesizing Enzymes															
Protein	estimate	std.error	statistic	p.value	Adjusted_P	R_squared	Adj_R_squared	R_delta	AIC	BIC	conf.low	conf.high	Condition	SampleSize	Predictors
GPX4	0,518492	0,196674	2,636303	0,011873	0,047492883	0,184913	0,12378096	0,117276	133,5168	142,4378	0,120999	0,915985	high AIFM2	44	GPX4, AIFM2, SLC7A11
GPX4	0,413072	0,182462	2,263873	0,029076	0,058152502	0,229998	0,172248064	0,096196	131,0131	139,934	0,044301	0,781842	high AIFM2	44	GPX4, AIFM2, MPST
MPST	0,524386	0,211412	2,480406	0,01743	0,058152502	0,229998	0,172248064	0,122983	131,0131	139,934	0,097108	0,951665	high AIFM2	44	GPX4, AIFM2, MPST

Table 4. Multiple Linear Regression (MLR) analysis results for Erastin resistance models using SLC7A11, TST, MPST, GPX4, and AIFM2 as independent variables in Negligible AIFM2 cell subsets. Red and Blue cells highlight unique combination of condition and predictor set which represents an independent model.

Negligible AIFM2 Cell Set Multiple Linear Regression Models for Erastin Resistance vs Protein Expression of Ferroptosis Inhibitors and Known Persulfide Synthesizing Enzymes															
Protein	estimate	std.error	statistic	p.value	Adjusted_P	R_squared	Adj_R_squared	R_delta	AIC	BIC	conf.low	conf.high	Condition	SampleSize	Predictors
GPX4	0,737374	0,186315	3,957661	0,00033	0,001320824	0,333479	0,279437017	0,304218	105,4847	114,0526	0,359863	1,114885	negligible AIFM2	41	GPX4, AIFM2, SLC7A11
GPX4	0,771333	0,183908	4,194129	0,000164	0,000656035	0,325279	0,270571525	0,32226	105,9861	114,5539	0,3987	1,143965	negligible AIFM2	41	GPX4, AIFM2, TST
GPX4	0,773163	0,18934	4,083463	0,000228	0,000911573	0,324196	0,269401073	0,31472	106,0518	114,6197	0,389524	1,156803	negligible AIFM2	41	GPX4, AIFM2, MPST

Table 5. Multiple Linear Regression (MLR) analysis results for Erastin resistance models using SLC7A11, TST, GPX4, and AIFM2 as independent variables in Both Low cell subsets. Red cells highlight unique combination of condition and predictor set which represents an independent model.

Both Low(GPX4&AIFM2) Cell Set Multiple Linear Regression Models for Erastin Resistance vs Protein Expression of Ferroptosis Inhibitors and Known Persulfide Synthesizing Enzymes															
Protein	estimate	std.error	statistic	p.value	Adjusted_P	R_squared	Adj_R_squared	R_delta	AIC	BIC	conf.low	conf.high	Condition	SampleSize	Predictors
AIFM2	0,538257	0,229582	2,344512	0,023237	0,058199704	0,239267	0,175872531	0,08804	179,882	191,7038	0,076652	0,999862	both low	53	GPX4, AIFM2, SLC7A11, TST
TST	0,456808	0,194906	2,343741	0,02328	0,058199704	0,239267	0,175872531	0,086925	179,882	191,7038	0,064924	0,848692	both low	53	GPX4, AIFM2, SLC7A11, TST

Table 6. Multiple Linear Regression (MLR) analysis results for Erastin resistance models using SLC7A11, TST, MPST, GPX4, and AIFM2 as independent variables in All cell subsets. Red and Blue cells highlight unique combination of condition and predictor set which represents an independent model.

All Cell Set Multiple Linear Regression Models for Erastin Resistance vs Protein Expression of Ferroptosis Inhibitors and Known Persulfide Synthesizing Enzymes															
Protein	estimate	std.error	statistic	p.value	Adjusted_P	R_squared	Adj_R_squared	R_delta	AIC	BIC	conf.low	conf.high	Condition	SampleSize	Predictors
GPX4	0,317951	0,084172	3,777404	0,000199	0,000993186	0,116409	0,102100142	0,034166	743,014	764,1906	0,152165	0,483737	all	252	GPX4, AIFM2, SLC7A11, TST
AIFM2	0,191944	0,063907	3,003466	0,002944	0,007358921	0,116409	0,102100142	0,032043	743,014	764,1906	0,066071	0,317817	all	252	GPX4, AIFM2, SLC7A11, TST
SLC7A11	0,155754	0,059424	2,621075	0,009309	0,015515071	0,116409	0,102100142	0,023073	743,014	764,1906	0,038712	0,272795	all	252	GPX4, AIFM2, SLC7A11, TST
TST	0,172864	0,068808	2,512257	0,012635	0,015793239	0,116409	0,102100142	0,027126	743,014	764,1906	0,037338	0,30839	all	252	GPX4, AIFM2, SLC7A11, TST
GPX4	0,277653	0,08667	3,203574	0,001536	0,003839554	0,104578	0,090076908	0,02757	746,366	767,5426	0,106947	0,448359	all	252	GPX4, AIFM2, SLC7A11, MPST
AIFM2	0,215014	0,063593	3,381078	0,000839	0,003839554	0,104578	0,090076908	0,036962	746,366	767,5426	0,089759	0,340268	all	252	GPX4, AIFM2, SLC7A11, MPST
SLC7A11	0,153605	0,059998	2,560169	0,011058	0,018430167	0,104578	0,090076908	0,023199	746,366	767,5426	0,035432	0,271779	all	252	GPX4, AIFM2, SLC7A11, MPST

A

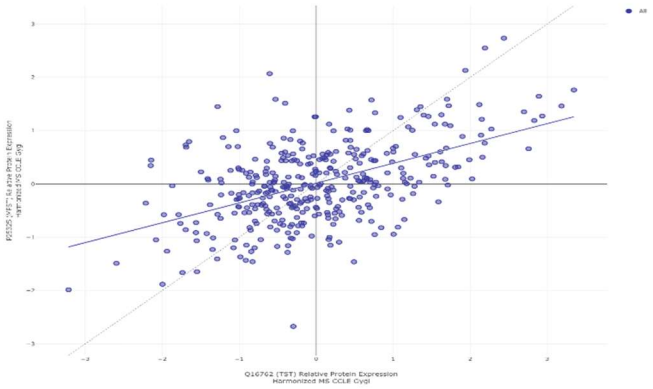

Points	Pearson	Spearman	Slope	Intercept	p-value (linregress)
375	0.513	0.436	3.72E-1	1.54E-2	1.37E-26

B

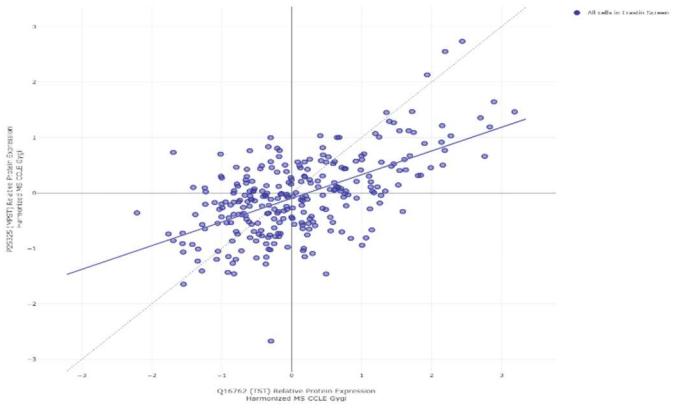

Group	Points	Pearson	Spearman	Slope	Intercept	p-value (linregress)
All cells in Erastin Screen	276	0.588	0.518	4.27E-1	-9.68E-2	5.13E-27

Figure 3. Corallation & SLR analyses generated using the DepMap Portal Plot Configuration tool.
A. The Scatterplot results of the corelation and SLR between TST expression and MPST expression across all cell lines in the CCLE proteomics dataset B. The Scatterplot results of the corelation and LR between TST expression and MPST expression across cell lines both in the CCLE proteomics dataset and Erastin Drug Screen in the PRISM Repurposing Public 24Q2 dataset

6.0 Interpretation

TST, MPST, SLC7A11, GPX4, and AIFM2 each show statistically significant, though varying, positive associations with Erastin resistance across cancer cell lines. These associations differ by molecular context, with some effects enhanced in specific subgroups defined by GPX4 and AIFM2 expression levels. Importantly, while the stratified subgroup MLR models are not statistically independent—due to overlapping samples—they remain analytically distinct, as they aim to uncover context-specific effects. In this sense, the models test interaction-like behaviors, such as:

- *Does a persulfide synthesizing protein's correlation with resistance become stronger when GPX4 is low?*
- *Is the effect of TST only apparent within certain expression contexts?*

Corelation & SLR analysis results:

- *TST* shows only intermediate and significant correlation in negligible GPX4 and both AIFM2&GPX4 low subgroup (Pearson's r ≈ 0.32 in negligible GPX4 subgroup; ≈ 0.26 in both low subgroup). It also shows weak but statistically significant positive correlation with Erastin resistance in other subgroup conditions (Pearson's r ≈ 0.17, p ≈ 0.04 across all samples; Pearson's r ≈ 0.20, p ≈ 0.009 in the low GPX4 subgroup) (Table 1, Figure 1B).
- *MPST* exhibits a moderate correlation (Pearson's r ≈ 0.16–0.36), most notable in the high AIFM2 subgroup (Pearson's r ≈ 0.37, p ≈ 0.014), suggesting functional synergy with AIFM2 (Table 1, Figure 1a).
- *SLC7A11* shows weak but consistent positive correlations across subgroups (Pearson's r ≈ 0.13–0.15), supporting its role in ferroptosis regulation through cystine import.
- *GPX4* and *AIFM2* generally show the strongest individual correlations with Erastin resistance, consistent with their established roles as core ferroptosis inhibitors.

Stratified multiple linear regression (MLR) models:

- In the low GPX4 condition:
    - TST (β ≈ 0.17, p ≈ 0.02) and MPST (β ≈ 0.19, p ≈ 0.06) each contribute positively to resistance (Table 2).
    - AIFM2 remains the strongest predictor (β ≈ 0.28–0.26, p < 0.001), with relatively high explanatory power (R^2 ≈ 0.129–0.12, ΔR ≈ 0.07–0.06) (Table 2).
    - SLC7A11 shows a weak but statistically significant association with resistance in both the low GPX4(β ≈ 0.13–0.15, p ≈ 0.03–0.04) and all groups (β ≈ 0.15, p ≈ 0.015–0.018) (Table 2 & 6). While its contribution is smaller than that of AIFM2 or MPST, this effect is biologically plausible given SLC7A11's role in cystine import and redox regulation.
- In the high AIFM2 subgroup:
    - MPST shows a strong independent effect (β ≈ 0.52, p ≈ 0.013), explaining over 55% of the model's R^2, suggesting a synergistic role with AIFM2 in promoting resistance (Table 3, Figures 2b and 2c).
- In the negligible AIFM2 group:

        - GPX4 dominates the resistance phenotype, accounting for >97% of model variance, indicating that in the absence of AIFM2, GPX4 is the primary determinant (Table 4, Figures 2b and 2c).

- In all and both low groups:
    - In the full dataset (all subgroup) GPX4 consistently exhibited the strongest effect on Erastin resistance, followed by AIFM2, as expected. While TST and MPST also showed weak but statistically significant associations, the overall low R^2 values (≈0.10–0.09) suggest these models explain only a limited portion of the resistance variance indicating the existence of more complex and nonlinear systems promoting erastin resistance and sensitivity overall (Table 6, Figure 2C).
    - Notably, in the low-GPX4 and low-AIFM2 subgroup—despite a smaller but still robust sample size—the TST model demonstrated improved explanatory power ($R^2 \approx 0.17$), with both AIFM2 ($\beta \approx 0.53$, $p \approx 0.058$) and TST ($\beta \approx 0.45$, $p \approx 0.058$) showing strong, significant positive effects. While adjusted p value is not exactly under the consensus threshold of 0.05, it is close enough to be assessed as an indication of a potentially synergistic role under conditions of dual suppression in key ferroptosis regulators. A further study with higher sample volume would be plausible to verify this effect (Table 5).

Across both linear and stratified MLR models, TST and MPST are consistently associated with increased Erastin resistance, particularly under low GPX4 expression (Figure 2A, Table 1 & 2). SLC7A11 shows a weak but statistically significant effect in the low GPX4 and full-sample models, suggesting a modest role in modulating ferroptosis perhaps via redox balance (Figure 2A). MPST exhibits a strong, AIFM2-dependent effect, especially in the high AIFM2 subgroup, where it accounts for the majority of model explanatory power (Figure 2A). In contrast, TST maintains a weaker but more broadly distributed effect, including in the low GPX4, low AIFM2, and both low subgroups, highlighting potential differences in how these enzymes contribute to ferroptosis resistance (Figure 2A, Table 1, 3, 5).

Additionally, the revealed a positive correlation between TST expression and erastin resistance within the both low subgroup in correlation and LR analysis also supported by MLR, supporting the hypothesis that TST may function more broadly across ferroptosis contexts, while MPST's effect appears more AIFM2-dependent (Table 1, Figure 1, Table 5).

7.0 Conclusion

While these results do not establish whether SLC7A11, TST, and MPST actively mediate ferroptosis resistance or merely serve as correlated markers within shared metabolic or regulatory pathways, they provide a foundational landscape of their associations with Erastin resistance across diverse cancer cell types. This global profile lays the groundwork for targeted functional studies and, when combined with lineage-specific analyses, could help identify tumor-type–specific dependencies and clarify the broader biological relevance of these associations.

Notably, all correlations in this study were based on basal (pre-treatment) protein expression levels. Since gene and protein expression in cancer cells is highly dynamic and responsive to environmental stimuli, including drug exposure, the associations identified here may not fully reflect treatment-

induced regulatory mechanisms. For example, the absence of a clear CBS–Erastin resistance correlation in stratified linear regression models may indicate that CBS acts as a context-dependent or inducible ferroptosis suppressor, rather than one constitutively expressed at functionally relevant levels across cancer types.

To overcome this limitation, future studies could incorporate dynamic expression profiling, capturing protein level changes before and after Erastin exposure. While scaling such an approach to the level of the DepMap proteomics dataset—which quantified thousands of proteins via mass spectrometry across 375 cell lines (Gygi Lab, Viswanathan et al., 2020)—would be logistically and financially demanding, focused follow-up studies using a curated subset of cell lines, or patient-derived xenograft or organoid models, may yield more feasible and clinically actionable insights. These targeted approaches could be particularly informative for highlighting the synergistic roles of GPX4, AIFM2, and downstream persulfide pathway components in ferroptosis resistance.

8.0 References:

1- Viswanathan, V. S., Ryan, M. J., Dhruv, H. D., Gill, S., Eichhoff, O. M., Seashore-Ludlow, B., ... & Stockwell, B. R. (2020). Dependency of a therapy-resistant state of cancer cells on a lipid peroxidase pathway. Cell, 181(5), 1046–1061.e21. https://doi.org/10.1016/j.cell.2020.04.040

2- Lu, B., Chen, X., Hong, Y., Zhu, H., He, Q., Yang, B., Ying, M., & Cao, J. (2019). Identification of PRDX6 as a regulator of ferroptosis. Acta Pharmacologica Sinica, 40(10), 1334–1342. https://doi.org/10.1038/s41401-019-0233-9

3- Berndt, C., Alborzinia, H., Amen, V. S., Ayton, S., Barayeu, U., Bartelt, A., Bayir, H., Bebber, C. M., Birsoy, K., Böttcher, J. P., Brabletz, S., Brabletz, T., Brown, A. R., Brüne, B., Bulli, G., Bruneau, A., Chen, Q., DeNicola, G. M., Dick, T. P., … Conrad, M. (2024). Ferroptosis in health and disease. Redox Biology, 75, 103211. https://doi.org/10.1016/j.redox.2024.103211

4- Chen, Z., Inague, A., Kaushal, K., Fazeli, G., N Xavier da Silva, T., Ferreira dos Santos, A., Cheytan, T., Porto Freitas, F., Yildiz, U., Gasparello Viviani, L., Santiago Lima, R., Peglow Pinz, M., Medeiros, I., Geronimo Pires Alegria, T., Pereira da Silva, R., Regina Diniz, L., Weinzweig, S., Klein-Seetharaman, J., Trumpp, A., … Friedmann Angeli, J. P. (2024). PRDX6 Contributes to Selenocysteine Metabolism and Ferroptosis Resistance. https://doi.org/10.1101/2024.06.04.597364

5- Adamiec-Organisciok, M., Wegrzyn, M., Cienciala, L., Sojka, D., Nackiewicz, J., & Skonieczna, M. (2023). Compensative resistance to Erastin-induced ferroptosis in GPX4 knock-out mutants in HCT116 cell lines. Pharmaceuticals, 16(12), 1710. https://doi.org/10.3390/ph16121710

6- Erdélyi, K., Ditrói, T., Johansson, H. J., Czikora, Á., Balog, N., Silwal-Pandit, L., Ida, T., Olasz, J., Hajdú, D., Mátrai, Z., Csuka, O., Uchida, K., Tóvári, J., Engebraten, O., Akaike, T., Børresen Dale, A.-L., Kásler, M., Lehtiö, J., & Nagy, P. (2021). Reprogrammed transsulfuration promotes basal-like breast tumor progression via realigning cellular cysteine persulfidation. Proceedings of the National Academy of Sciences, 118(45). https://doi.org/10.1073/pnas.2100050118

7- Zhang, C., Liu, X., Jin, S., Chen, Y., & Guo, R. (2022). Ferroptosis in cancer therapy: A novel approach to reversing drug resistance. Molecular Cancer, 21(1). https://doi.org/10.1186/s12943-022-01530-y

8- Diao, J., Jia, Y., Dai, E., Liu, J., Kang, R., Tang, D., Han, L., Zhong, Y., & Meng, L. (2024). Ferroptotic therapy in cancer: Benefits, side effects, and risks. Molecular Cancer, 23(1). https://doi.org/10.1186/s12943-024-01999-9

9- Wu, Z., Barayeu, U., Schilling, D., Dick, T. P., & Pratt, D. A. (2023). Emergence of (hydro)persulfides as suppressors of lipid peroxidation and ferroptotic cell death. Current Opinion in Chemical Biology, 76, 102353. https://doi.org/10.1016/j.cbpa.2023.102353
10- Barayeu, U., Schilling, D., Eid, M., Xavier da Silva, T. N., Schlicker, L., Mitreska, N., Zapp, C., Gräter, F., Miller, A. K., Kappl, R., Schulze, A., Friedmann Angeli, J. P., & Dick, T. P. (2022). Hydropersulfides inhibit lipid peroxidation and ferroptosis by scavenging radicals. Nature Chemical Biology, 19(1), 28–37. https://doi.org/10.1038/s41589-022-01145-w
11- Corsello, S. M., Nagari, R. T., Spangler, R. D., Rossen, J., Kocak, M., Bryan, J. G., Humeidi, R., Peck, D., Wu, X., Tang, A. A., Wang, V. M., Bender, S. A., Lemire, E., Narayan, R., Montgomery, P., Ben-David, U., Garvie, C. W., Chen, Y., Rees, M. G., … Golub, T. R. (2020). Discovering the anticancer potential of non-oncology drugs by systematic viability profiling. *Nature Cancer*, *1*(2), 235–248. https://doi.org/10.1038/s43018-019-0018-6
12- Nusinow, D. P., Szpyt, J., Ghandi, M., Rose, C. M., McDonald, E. R., Kalocsay, M., Jané-Valbuena, J., Gelfand, E., Schweppe, D. K., Jedrychowski, M., Golji, J., Porter, D. A., Rejtar, T., Wang, Y. K., Kryukov, G. V., Stegmeier, F., Erickson, B. K., Garraway, L. A., Sellers, W. R., & Gygi, S. P. (2020). Quantitative proteomics of the Cancer Cell Line Encyclopedia. *Cell*, *180*(2). https://doi.org/10.1016/j.cell.2019.12.023